Chinese Chemical Letters 36 (2025) 110836

Contents lists available at ScienceDirect

Chinese Chemical Letters

journal homepage: www.elsevier.com/locate/cclet

Microenvironment regulation of copper sites by chelating hydrophobic polymer for electrosynthesis of ethylene

Lei Zhang[a,b,*], Chenyang Kou[a], Kun Ni[a], Yiwen Chen[c], Tongchuan Zhang[a], Baoliang Zhang[a,*]

[a] School of Chemistry and Chemical Engineering, Northwestern Polytechnical University, Xi'an 710129, China
[b] Research & Development Institute of Northwestern Polytechnical University in Shenzhen, Shenzhen 518063, China
[c] Queen Mary University of London Engineering School, Northwestern Polytechnical University, Xi'an 710129, China

ARTICLE INFO

Article history:
Received 24 November 2024
Revised 8 January 2025
Accepted 8 January 2025
Available online 9 January 2025

Keywords:
Molecular catalyst
Microenvironment regulation
Electrocatalytic acetylene semihydrogenation
Faradaic efficiency

ABSTRACT

Molecular catalysts can effectively steer the electrocatalytic acetylene semihydrogenation into ethylene, but realizing high Faradaic efficiency (FE) at industrial current densities remains a challenge. Herein, we report a ligand engineering strategy that utilizes polymeric *N*–heterocyclic carbene (NHC) as a hydrophobic ligand to modulate the microenvironment of Cu sites. This polymeric NHC imparts appropriate hydrophobic properties for the chelated Cu sites, thereby moderating the H_2O transport and enabling easy access of acetylene. Consequently, the polymeric NHC chelated Cu exhibits an $FE_{ethylene}$ of ~97% at a current density of 500 mA/cm^2 in a flow cell. Particularly in a zero-gap reactor, the $FE_{ethylene}$ consistently exceeds 86% across current densities from 100 mA/cm^2 to 400 mA/cm^2, reaching an optimal $FE_{ethylene}$ of 98% at 200 mA/cm^2 and achieving durable operation for 155 h at 100 mA/cm^2. This work provides a promising paradigm to regulate the microenvironment of molecular catalysts for improving electrocatalytic performances under industrial current densities.

Ethylene is among the most produced commodity chemicals for the polymer industry, predominantly made from steam cracking of liquefied petroleum gas [1]. Electrocatalytic semihydrogenation, combined with coal-derived acetylene, affords a petroleum-independent route to produce ethylene utilizing water (H_2O) as a proton source under ambient conditions [2]. Here, electrocatalysts driven this semihydrogenation process towards the desired ethylene product while minimizing the formation of by-products [3–5].

Copper (Cu) represents a promising metal for electrocatalytic acetylene semihydrogenation (EAH) because of its favorable properties in acetylene absorption and ethylene desorption [6]. To date, various design strategies, including unsaturated/undercoordinated sites [7,8], heteroatom doping [9], single atom [10,11], ligand engineering [12,13], bimetallic sites [14–16], structure/facet engineering [17,18], have been proposed to enhance the EAH performance of Cu-based catalysts. Among them, ligand engineering is an effective yet underexplored strategy for Cu-based catalysts. Cu-based molecular catalysts offer well-defined Cu sites with controllable coordination environments, enabling the fine-tuning of catalytic performance through ligand engineering. Nevertheless, most reported molecular catalysts for EAH operate at current densities below 200 mA/cm^2, which falls short of the profitability threshold that requires Faradaic efficiencies of ethylene ($FE_{ethylene}$) above 85% at current densities ≥200 mA/cm^2 [7]. Moreover, molecular catalysts that satisfy this profitability threshold in a zero-gap reactor remain unexplored for EAH.

In this regard, we reported a ligand engineering strategy that utilized polymeric *N*–heterocyclic carbene (NHC) as a hydrophobic ligand to modulate the microenvironment of Cu sites. Molecular dynamics (MD) simulations and experimental results demonstrated that polymeric NHC endowed the chelated Cu sites with appropriate hydrophobic character, which slowed down H_2O transport and allowed acetylene to access the Cu sites easily. Accordingly, the polymeric NHC chelated Cu (IOP-NHC Cu) exhibited remarkable EAH performance in a flow cell, with an $FE_{ethylene}$ of ~97% at a current density of 500 mA/cm^2. Especially in a zero-gap reactor, IOP-NHC Cu kept the $FE_{ethylene}$ exceeding 86% across current densities from 100 mA/cm^2 to 400 mA/cm^2, realizing an optimal $FE_{ethylene}$ of 98% at 200 mA/cm^2 ($E_{cell} = -2.5$ V). Additionally, IOP-NHC Cu substantiated exceptional stability, sustaining an

* Corresponding authors.
E-mail addresses: leizhang@nwpu.edu.cn (L. Zhang), blzhang@nwpu.edu.cn (B. Zhang).

https://doi.org/10.1016/j.cclet.2025.110836
1001-8417/

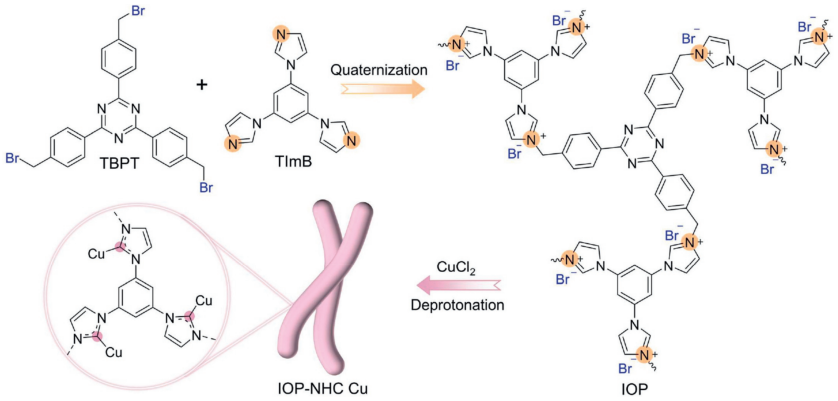

Fig. 1. Schematic illustration for the synthesis of IOP-NHC Cu.

$FE_{ethylene}$ >90% and steady E_{cell} over 155 h of continuous operation at 100 mA/cm^2. These results surpassed the performance of most reported molecular catalysts for EAH to a significant extent.

As depicted in Fig. 1, IOP-NHC Cu was synthesized *via* quaternization and deprotonation processes. Specifically, imidazolium-based organic polymer (IOP) was first prepared through quaternization of 2,4,6-tris(4-(bromomethyl)phenyl)–1,3,5-triazine (TBPT, Fig. S1a in Supporting information) with 1,3,5-tri(1*H*-imidazol-1-yl)benzene (TImB, Fig. S1b in Supporting information). The structure of resulting IOP was characterized by scanning electron microscopy (SEM), transmission electron microscopy (TEM) and X-ray diffraction (XRD) pattern. These results evidenced that IOP had a nanofiber morphology with homogeneous distribution of C, N and Br elements (Figs. S2 and S3 in Supporting information) as well as an amorphous crystal structure (Fig. S4 in Supporting information). As the Fourier transform infrared (FT-IR) spectra shown in Fig. S5 (Supporting information), -C-Br stretching vibration of TBPT at 601 cm^{-1} disappeared for IOP [19], indicating the complete quaternization of TBPT and TImB. Also, solid-state carbon nuclear magnetic resonance (^{13}C ssNMR) spectra of IOP possessed distinct peaks of triazine, methylene and aromatic carbons deriving from TBPT and TImB (Fig. S6 in Supporting information).

Subsequently, the deprotonation of IOP with copper precursor and potassium *tert*–butoxide (*t*-BuOK) yielded the IOP-NHC Cu. As observed in Fig. S7 (Supporting information), IOP-NHC Cu featured uniformly distributed Cu sites, while preserving the morphology characteristics of IOP nanofibers. Meanwhile, Cu sites are chelated into IOP without affecting its amorphous in nature (Fig. S8 in Supporting information). By comparing the FT-IR spectra of IOP and IOP-NHC Cu (Fig. 2a), a distinctive IR peak representing C–N stretching vibration of NHC emerged at 1262 cm^{-1} for IOP-NHC Cu [20], whereas its C–N$^+$ stretching band of imidazolium ring at 1222 cm^{-1} decreased significantly [21]. This result signified the formation of IOP-NHC Cu based on IOP. Besides, X-ray photoelectron spectra (XPS) of IOP and IOP-NHC Cu were performed to investigate their chemical composition (Fig. S9 in Supporting information). As displayed in Fig. 2b, the N 1s spectrum of IOP was deconvolved into distinct N 1s peaks with imidazolium at 401.7 eV and triazine at 398.8 eV [22]. Notably, the N 1s peak at 401.7 eV for IOP was negatively shifted to 401.2 eV for IOP-NHC Cu, similar to the behavior of N 1s spectra for imidazolium-derived NHC on metal sites [23,24]. Furthermore, the Cu $2p_{3/2}$ spectrum of IOP-NHC Cu exhibited two characteristic peaks at the binding energy of 932.2 eV and 934.5 eV (Fig. 2c), while the Cu LMM Auger spectra displayed peaks at 571.4 eV and 569.9 eV (Fig. S10 in Supporting information), corresponding to the chelated Cu^{I} and Cu^{II} sites [25–28]. The thermogravimetric analysis (TGA) revealed weight losses

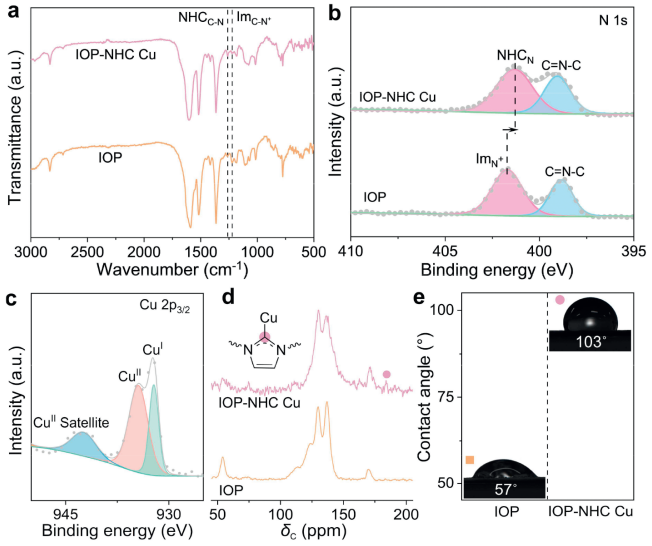

Fig. 2. Spectroscopic characterizations of IOP-NHC Cu. (a) FT-IR spectra of IOP and IOP-NHC Cu. (b) The deconvolution spectra of N 1s for IOP and IOP-NHC Cu. (c) The Cu $2p_{3/2}$ fitting results of IOP-NHC Cu. (d) ^{13}C ssNMR spectra of IOP and IOP-NHC Cu. (e) Contact angle measurements on IOP-NHC Cu and IOP electrodes.

of 60 wt% for IOP and 51 wt% for IOP-NHC Cu at 800 °C relative to their initial masses (Fig. S11 in Supporting information). Therein, IOP-NHC Cu had a smaller weight loss compared to IOP, also implying the successful chelation of Cu sites within IOP-NHC Cu. Combined with ^{13}C ssNMR results of IOP and IOP-NHC Cu (Fig. 2d), the existence of Cu-C bond at 184 ppm in IOP-NHC Cu further confirmed the chelation of Cu sites with carbenic carbon deriving from imidazolium of IOP [29–31]. Additionally, contact angle (CA) experiments were conducted on electrodes to investigate the microenvironment of IOP-NHC Cu and IOP as electrocatalysts by using 1 mol/L KOH electrolyte (Fig. 2e). Obviously, the CA of electrolyte increased from IOP (57°) to IOP-NHC Cu (103°), showcasing a more hydrophobic surface for IOP-NHC Cu. This characteristic is typically unfavorable for the hydrogen evolution reaction (HER) [32,33], thereby predicting the optimal accessibility of C_2H_2 toward the IOP-NHC Cu during EAH.

To verify the merits of IOP-NHC Cu for EAH, IOP-Cu was selected as the benchmark electrocatalyst, prepared by physically absorbing the same amount of Cu sites onto IOP. As characterized by SEM, TEM, HAADF-STEM, XRD and TGA analysis (Figs. S12–S15 in Supporting information), the morphology, composition and amor-

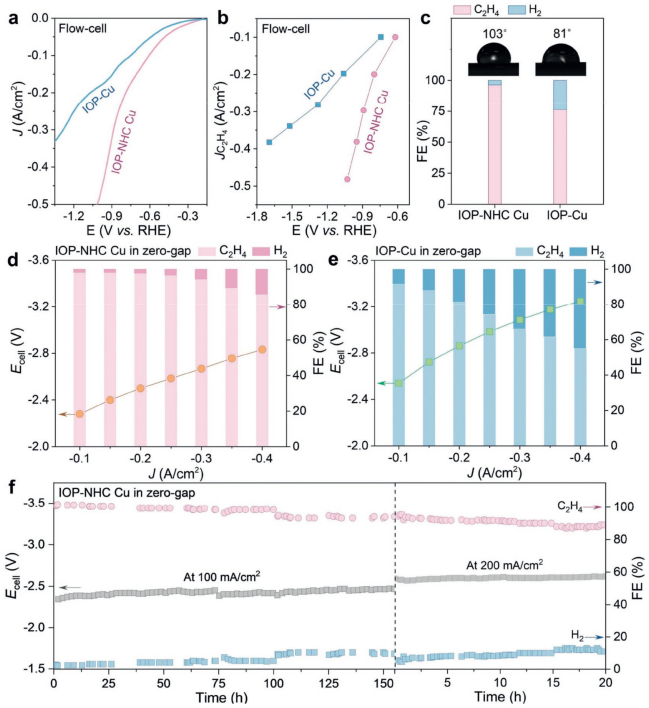

Fig. 3. EAH performances in (a-c) a flow cell and (d-f) a zero-gap reactor. (a) Polarization curves, (b) ethylene partial current densities, (c) product FEs at 500 mA/cm^2 of IOP-NHC Cu and IOP-Cu in 1 mol/L KOH aqueous solution under an acetylene stream. Inset of (c) was corresponding contact angle measurements for IOP-NHC Cu and IOP-Cu. E_{cell} and corresponding FEs as a function of current densities for (d) IOP-NHC Cu and (e) IOP-Cu using 1 mol/L KOH anolyte with 50 sccm humidified acetylene flow in the cathode. (f) Long-term stability of IOP-NHC Cu for the continuous semihydrogenation of humidified acetylene flow at cathodic current densities of 100 mA/cm^2 and 200 mA/cm^2.

phous structure of IOP-Cu were identical to those of IOP-NHC Cu. Unlike IOP-NHC Cu, no chelated Cu sites were observed in the FT-IR and ^{13}C ssNMR spectra of IOP-Cu (Figs. S16 and S17 in Supporting information), confirming that the Cu sites in IOP-Cu were merely physically absorbed. Next, the EAH performance of IOP-NHC Cu and IOP-Cu were assessed in 1 mol/L KOH electrolyte using a custom-made flow cell (Fig. S18 in Supporting information). The cathodic polarization curves displayed that the current density of IOP-NHC Cu in acetylene was significantly higher than that in argon (Fig. S19 in Supporting information), highlighting superior electrocatalytic activity towards acetylene. Remarkably, the current density of IOP-Cu at −1 V *vs.* RHE (187 mA/cm^2) was substantially lower than the 495 mA/cm^2 achieved by IOP-NHC Cu (Fig. 3a). Also, IOP-NHC Cu exhibited significantly higher ethylene partial current densities ($J_{C_2H_4}$) compared to IOP-Cu across the potential range from −0.6 V to −1.8 V (Fig. 3b). Correspondingly, IOP-NHC Cu achieved a maximum $J_{C_2H_4}$ of 485 mA/cm^2 at −1.03 V. Notably, IOP-NHC Cu possessed ethylene Faradaic efficiency ($FE_{ethylene}$) of >95% at current densities from 100 mA/cm^2 to 500 mA/cm^2 (Fig. S20 in Supporting information). Especially at 500 mA/cm^2, $FE_{ethylene}$ of IOP-NHC Cu was nearly 97% while the $FE_{ethylene}$ for IOP-Cu was 74% (Fig. 3c), which was in accordance with the CA results of IOP-NHC Cu (103°) and IOP-Cu (81°). This indicated that polymer-chelated Cu sites within IOP-NHC Cu possessed appropriate hydrophobicity, hence effectively suppressing the HER [34]. To this end, we further conducted control experiments on small molecule-chelated Cu sites (chloro(1,3-dimesitylimidazol-2-ylidene)copper, denoted as NHC–Cu) to verify whether the improved performance of IOP-NHC Cu benefiting from polymer-chelated Cu sites. As expected, IOP-NHC Cu completely outperformed NHC–Cu in terms of current density, $J_{C_2H_4}$ and $FE_{ethylene}$ (Fig. S21 in Supporting information). Moreover, IOP made a minimal contribution to $FE_{ethylene}$ (Fig. S22 in Supporting information), unambiguously demonstrating the dominant role of polymer-chelated Cu sites in promoting EAH.

In addition, we explored the full-cell EAH performance of IOP-NHC Cu as the cathode in a zero-gap reactor using humidified acetylene as the feed gas, wherein iridium oxide supported on titanium mesh (IrO_2/Ti mesh) as the anode for oxygen evolution reaction (Fig. S23 in Supporting information). As demonstrated in Fig. 3d, the current density of IOP-NHC Cu increased from 100 mA/cm^2 to 400 mA/cm^2 at the full-cell voltage (E_{cell}) range of −2.28 V to −2.83 V (without *iR* compensation). Concurrently, IOP-NHC Cu retained ≥86% of $FE_{ethylene}$ between E_{cell} of −2.28 V and −2.83 V, reaching an optimal $FE_{ethylene}$ of 98% at a current density of 200 mA/cm^2 (E_{cell} = −2.5 V). IOP-NHC Cu delivered a full-cell energy efficiency of ethylene ($EE_{ethylene}$) of 21.5%, with a current density of 100 mA/cm^2 at a E_{cell} of −2.28 V. In contrast, the $FE_{ethylene}$ and E_{cell} of IOP-Cu were inferior to those of IOP-NHC Cu under the same conditions (Fig. 3e). Particularly at 400 mA/cm^2, IOP-NHC Cu maintained 86% of $FE_{ethylene}$ with a relatively low E_{cell} of −2.83 V, whereas the $FE_{ethylene}$ of IOP-Cu decayed to 55% with a high E_{cell} of −3.25 V. In addition, the exceptional stability of IOP-NHC Cu in the zero-gap reactor was demonstrated in Fig. 3f, showing continuous operation at current densities of 100 mA/cm^2 for 155 h and 200 mA/cm^2 for 20 h, simultaneously maintaining ≥90% of $FE_{ethylene}$ and steady E_{cell}. Furthermore, XRD pattern of IOP-NHC Cu after the stability test confirmed stable Cu sites without forming Cu clusters or NPs (Fig. S24 in Supporting information). The above results further solidified that IOP-NHC Cu favored EAH over HER. As compared in Tables S1 and S2 (Supporting information), the EAH performance of IOP-NHC Cu surpassed most previously reported molecular catalysts both in flow cell and full-cell configurations [12,13,35–37].

Given the differences in performance between IOP-Cu and IOP-NHC Cu, molecular dynamics (MD) simulations were performed at 300 K for 35 ps using a canonical ensemble to investigate the absorption of H_2O molecules on the catalyst surface during EAH. The analysis of molecular density along the z-direction unveiled significantly different distributions of H_2O on the surfaces of IOP-NHC Cu and IOP-Cu (Fig. 4a). Specifically, the counts of H_2O adsorbed on the surface of IOP-NHC Cu were distinctly lower relative to IOP-Cu (Fig. 4b), which contributed to the suppression of HER [38]. Since protons are mainly provided by water dissociation in an alkaline electrolyte, the water motion was subsequently probed and compared to understand the proton supply. The mean square displacement (MSD), representing the motion of water molecules, was 116.7 Å/ps on IOP-Cu and 63.8 Å/ps on IOP-NHC Cu (Fig. 4c). This result illustrated the relatively slow proton supply of IOP-NHC Cu. Besides, *in-situ* Raman measurements were conducted to gain molecule-level insight into the microenvironment of IOP-NHC Cu. As shown in Fig. 4d, -OH stretching peak at 3436 cm^{-1} representing the interfacial water was only observed at a relatively high potential of −0.6 V [39]. This evidenced sluggish H_2O coverage on IOP-NHC Cu, in agreement with the MD simulation results. Moreover, in comparison with characteristic peaks of IOP-NHC Cu observed in the *in-situ* electrochemical Raman cell, a Raman peak associated with -C≡C- stretching vibration of acetylene (1918 cm^{-1}) was detected from the open circuit potential (OCP) to −0.6 V, confirming the adsorption of acetylene on IOP-NHC Cu [3]. Besides, the increase in potential led to a noticeable disparity in the peak area of -C=C- stretching vibration at 1558 cm^{-1} [40], indicating that IOP-NHC Cu favored the acetylene semihydrogenation into ethylene.

In summary, we developed polymeric NHC as a hydrophobic ligand to chelate Cu sites, thereby optimizing the microenvironment around the catalyst surface. This ligand engineering strategy created suitable accessibility of acetylene and H_2O, which facilitated the acetylene semihydrogenation into ethylene and guaran-

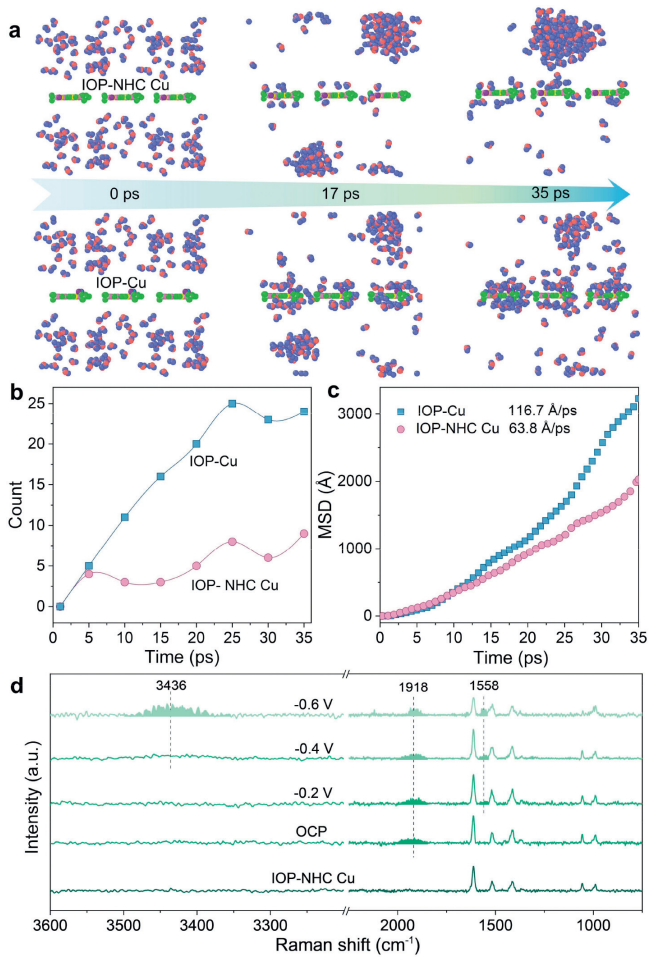

Fig. 4. (a) Molecular dynamics simulation snapshots of H_2O diffusion near the IOP-NHC Cu and IOP-Cu surfaces during 35 ps. (b) The number of surface H_2O near the IOP-NHC Cu and IOP-Cu surfaces during 35 ps. (c) Analysis of the mean square displacements of H_2O at the surface of IOP-NHC Cu and IOP-Cu. (d) *In-situ* electrochemical Raman spectra of IOP-NHC Cu for acetylene semihydrogenation in 1 mol/L KOH solution.

teed the EAH stability. As a result, IOP-NHC Cu demonstrated impressive performance with an $FE_{ethylene}$ of ~97% at a current density of 500 mA/cm^2 in a flow cell. Furthermore, in a zero-gap reactor, IOP-NHC Cu maintained an $FE_{ethylene}$ above 86% across current densities from 100 mA/cm^2 to 400 mA/cm^2, reaching a maximal $FE_{ethylene}$ of 98% at 200 mA/cm^2. More importantly, IOP-NHC Cu performed durablely and persisted ≥90% of $FE_{ethylene}$ at current densities of 100 mA/cm^2 for 155 h and 200 mA/cm^2 for 20 h. This work highlighted a polymeric ligand engineering strategy to regulate the microenvironment of molecular catalysts for enhancing EAH performances under industrial current densities.

Declaration of competing interest

The authors declare that they have no known competing financial interests or personal relationships that could have appeared to influence the work reported in this paper.

CRediT authorship contribution statement

Lei Zhang: Writing – review & editing, Writing – original draft, Funding acquisition, Formal analysis, Data curation. **Chenyang Kou:** Methodology, Data curation. **Kun Ni:** Formal analysis. **Yiwen Chen:** Data curation. **Tongchuan Zhang:** Methodology. **Baoliang Zhang:** Supervision, Funding acquisition.

Acknowledgments

This work was financially supported by the National Natural Science Foundation of China (Nos. 22475170, 52101271, 22375166), the Guangdong Basic and Applied Basic Research Foundation (Nos. 2020A1515111017, 2024A1515011977), and the Key Research and Development Program of Shaanxi Province (No. 2024GX-YBXM-379).

Supplementary materials

Supplementary material associated with this article can be found, in the online version, at doi:10.1016/j.cclet.2025.110836.

References

[1] H. Zimmermann, R. Walzl, Ethylene, Ullmann's Encyclopedia of Industrial Chemistry, Wiley, Hoboken, 2009.
[2] S. Wang, K. Uwakwe, L. Yu, et al., Nat. Commun. 12 (2021) 7072.
[3] J. Bu, Z. Liu, W. Ma, et al., Nat. Catal. 4 (2021) 557–564.
[4] R. Shi, Z. Wang, Y. Zhao, et al., Nat. Catal. 4 (2021) 565–574.
[5] S. Chang, J. Bu, J. Li, et al., Chin. Chem. Lett. 34 (2023) 107765.
[6] Z. Chen, C. Cai, T. Wang, J. Phys. Chem. C 126 (2022) 3037–3042.
[7] B.H. Zhao, F. Chen, M. Wang, et al., Nat. Sustain. 6 (2023) 827–837.
[8] W. Xue, X. Liu, C. Liu, et al., Nat. Commun. 14 (2023) 2137.
[9] L. Bai, Y. Wang, Z. Han, et al., Nat. Commun. 14 (2023) 8384.
[10] X. Jiang, L. Tang, L. Dong, et al., Angew. Chem. Int. Ed. 62 (2023) e202307848.
[11] Z. Wang, L. Shang, H. Yang, et al., Adv. Mater. 35 (2023) e2303818.
[12] L. Zhang, Z. Chen, Z. Liu, et al., Nat. Commun. 12 (2021) 6574.
[13] J. Li, Y. Guo, S. Chang, et al., Small 19 (2023) e2205845.
[14] C. Cheng, F. Chen, B. Zhang, et al., Angew. Chem. Int. Ed. 64 (2025) e202413897.
[15] Z. Wang, C. Li, G. Peng, et al., Angew. Chem. Int. Ed. 63 (2024) e202400122.
[16] X.H. Lv, H. Huang, L.T. Cui, et al., ACS Appl. Mater. Interfaces 16 (2024) 8668–8678.
[17] F. Chen, L. Li, C. Cheng, et al., Nat. Commun. 15 (2024) 5914.
[18] Z. Wu, J. Zhang, Q. Guan, et al., Adv. Mater. 36 (2024) e2408681.
[19] A. Chakraborty, S. Sarkar, P. Nag, et al., Mater. Chem. Front. 7 (2023) 1831–1840.
[20] M. Dabiri, S.I. Alavioon, S.K. Movahed, J. Iran. Chem. Soc. 15 (2018) 2463–2474.
[21] S. Bhattacharjee, A. Tripathi, R. Chatterjee, et al., ACS Catal. 14 (2024) 718–727.
[22] X. Fang, C. Liu, L. Yang, et al., J. CO2 Util. 54 (2021) 101778.
[23] A. Ruhling, K. Schaepe, L. Rakers, et al., Angew. Chem. Int. Ed. 55 (2016) 5856–5860.
[24] L.M. Martinez-Prieto, L. Rakers, A.M. Lopez-Vinasco, et al., Chem. Eur. J. 23 (2017) 12779–12786.
[25] K.H. Park, I. Ku, H.J. Kim, S.U. Son, Chem. Mater. 20 (2008) 1673–1675.
[26] S. Chen, W.H. Li, W. Jiang, et al., Angew. Chem. Int. Ed. 61 (2022) e202114450.
[27] M. Luo, A. Ozden, Z. Wang, et al., Adv. Mater. 35 (2023) e2209567.
[28] Y. Liu, H. Tang, Y. Zhou, B.L. Lin, Nano Res. 17 (2023) 3761–3768.
[29] N. Kaeffer, D. Mance, C. Coperet, Angew. Chem. Int. Ed. 59 (2020) 19999–20007.
[30] N. Kaeffer, H.J. Liu, H.K. Lo, et al., Chem. Sci. 9 (2018) 5366–5371.
[31] A.J. Veinot, A. Al-Rashed, J.D. Padmos, et al., Chem. Eur. J. 26 (2020) 11431–11434.
[32] T.H.M. Pham, J. Zhang, M. Li, et al., Adv. Energy Mater. 12 (2022) 2103663.
[33] J. Ryu, D.W. Lee, J. Mater. Chem. A 12 (2024) 10012–10043.
[34] Q. Luo, H. Duan, M.C. McLaughlin, et al., Chem. Sci. 14 (2023) 9664–9677.
[35] Z. Liu, Z. Chen, J. Bu, et al., Chem. Eng. J. 431 (2022) 134129.
[36] L. Zhang, R. Bai, J. Lin, et al., Nat. Chem. 16 (2024) 893–900.
[37] Z. Song, R. Yang, X. Liu, et al., Angew. Chem. Int. Ed. 63 (2024) e202410200.
[38] Q. Fan, P. Yan, F. Liu, et al., Sci. Bull. 69 (2024) 2881–2891.
[39] Z. Liu, X. Lv, S. Kong, et al., Angew. Chem. Int. Ed. 62 (2023) e202309319.
[40] W. Ma, Z. Chen, J. Bu, et al., J. Mater. Chem. A 10 (2022) 6122–6128.